Acta Cryst. (1997). A53, 781–788

Application of Grazing-Angle X-ray Standing Waves to the In-Plane Structure of a 100 Å-Thick Epilayer Film

O. SAKATA* AND H. HASHIZUME

Materials and Structure Laboratory, Tokyo Institute of Technology, Nagatsuta, Midori, Yokohama 226, Japan. E-mail: sakata1@rlem.titech.ac.jp

(*Received 25 February 1997; accepted 14 June 1997*)

Abstract

The grazing-angle X-ray standing-wave technique is applied to a 100 Å-thick $Ca_{0.39}Sr_{0.61}F_2$ epilayer film on a GaAs(111) substrate. Experimental data collected with the $(\bar{2}20)$ Bragg planes are explained by calculations taking into account dynamical diffraction in the thin film, but not by a homogeneous medium, only refracting and absorbing X-rays on the substrate. In this grazing-angle geometry, both X-ray penetration and extinction length are much smaller than in the conventional X-ray standing-wave geometry where epilayer diffraction does not significantly disturb the X-ray field produced by the bulk substrate. The results show that the epilayer (Ca, Sr)-atom planes perpendicular to the interface have laterally coincident positions with the $(\bar{2}20)$ atomic planes of the substrate GaAs within an experimental uncertainty of 2% of the lattice spacing. The coherent fraction of 66% observed for the epilayer suggests a disordered Sr-atom distribution in the in-plane direction, which is ascribed to combined effects of thermal vibration, interstitial atoms and interfacial dislocations. It is the first time, to the authors' knowledge, that the grazing-angle standing-wave technique has been applied to the structure determination of an epilayer film.

1. Introduction

The grazing-angle X-ray standing-wave (GAXSW) technique uses dynamical X-ray fields formed above a crystal surface when a beam, incident at a grazing angle, excites a specular and a diffracted beam from lattice planes perpendicular to the surface to determine the in-plane structure of overlayer atoms through observation of emission profiles (Cowan, 1985). The field intensity is modulated along the surface since the reciprocal-lattice vector is directed parallel to the surface. It is modulated in the surface-normal direction as well, but this is a long-period modulation. The technique was applied to arsenic-adsorbed silicon surfaces in a high-vacuum environment, demonstrating its capability to accurately determine the position and the ordering of adsorbed atoms on the bulk-like Si(111) surface (Sakata & Hashizume, 1995). There the arsenic emission intensity was proportional to the field strength of the GAXSW generated by the substrate silicon crystal. This was also the case in the earlier study on an iodine-adsorbed germanium surface in air (Jach & Bedzyk, 1990). We applied the technique to a 100 Å-thick epilayer $Ca_{0.39}Sr_{0.61}F_2$ film grown on a GaAs substrate but the observed Sr emission profiles could not be explained by a simple picture where the film emission is proportional to the substrate field intensity (Sakata, Kawamoto & Hashizume, 1992). Since the $Ca_{0.39}Sr_{0.61}F_2$ film is crystalline, with a lattice constant well matched with that of the substrate, and since the X-ray penetration is typically 100 Å at the glancing incidence angles used in the experiment, we thought that the exciting X-ray field was modified by a dynamical Bragg reflection inside the film. Our thought was supported by the small extinction distance calculated for $Ca_{0.39}Sr_{0.61}F_2$ in the grazing-angle geometry, which is comparable with the film thickness (Sakata & Hashizume, 1991).

The present paper describes a new analysis of the data presented by Sakata, Kawamoto & Hashizume (1992). We give a general discussion on GAXSW's in a system composed of an epilayer as thin as 100 Å and a perfect-crystal substrate. We provide an expression for GAXSW for this case and apply it to the $Ca_{0.39}Sr_{0.61}F_2$/GaAs system, to demonstrate our expression's validity and, at the same time, to analyze the sample structure. In §2, we present expressions for the field intensity in the epilayer–substrate system. Three models are considered for the interface structure of the system. In order to be self-contained, our sample and experiment are described in §3. The result, presented in §4, allows us to determine the registration of epilayer-atom planes on the substrate surface and their disorder.

2. Expression of GAXSW for epilayer–substrate systems

We treat a thin epilayer film grown on a substrate, assuming that both the film and the substrate are perfect crystals. Fig. 1 shows the waves in our grazing-angle diffraction geometry. A plane X-ray wave with σ polarization, $\mathbf{K}_0$, strikes a flat surface of the thin epilayer film of thickness t at grazing angle φ_0. It satisfies the Bragg condition on a set of lattice planes normal to the surface, $\Delta\theta = \theta - \theta_B \simeq 0$. For φ_0 close to the critical

© 1997 International Union of Crystallography
Printed in Great Britain – all rights reserved

angle for total external reflection, φ_c, a specular reflected wave $\mathbf{K}_S$ and a diffracted wave $\mathbf{K}_h$ emerge from the surface. Above the surface, the X-ray field is written as

$$E_0 \exp(-2\pi i\mathbf{K}_0 \cdot \mathbf{r}) + E_S \exp(-2\pi i\mathbf{K}_S \cdot \mathbf{r}) + E_h \exp(-2\pi i\mathbf{K}_h \cdot \mathbf{r}). \quad (1)$$

In the film, there are four pairs of waves generated: two pairs of transmitted and diffracted waves, denoted by $j = 1$ and 2, travel downwards and the other two pairs, denoted by $j = 3$ and 4, travel upwards from the film–substrate interface (Aleksandrov, Afanasyev & Stepanov, 1985; Sakata & Hashizume, 1991):

$$\sum_{j=1}^{4}[D_{oj}^{\text{epi}} \exp(-2\pi i\mathbf{k}_{oj}^{\text{epi}} \cdot \mathbf{r}) + D_{hj}^{\text{epi}} \exp(-2\pi i\mathbf{k}_{hj}^{\text{epi}} \cdot \mathbf{r})]. \quad (2)$$

Waves of $j = 1$ and 2 correspond to the two branches of the dispersion surface in the two-wave approximation of the dynamical diffraction theory, and waves of $j = 3$ and 4 are their reflections at the film–substrate boundary. It is defined that $\mathbf{k}_{o2}^{\text{epi}}$ has a larger vertical component than $\mathbf{k}_{o1}^{\text{epi}}$. The superscript $^{\text{epi}}$ denotes variables for the epilayer. Similarly, the superscript $^{\text{sub}}$ denotes variables for the substrate in the forthcoming expressions. The transmitted $\mathbf{k}_{oj}^{\text{epi}}$ and diffracted $\mathbf{k}_{hj}^{\text{epi}}$ waves (j = 1–4) are dynamically coupled to form four Bloch waves. These waves generate two transmitted and two diffracted waves in the substrate:

$$\sum_{j}^{2}[D_{oj}^{\text{sub}} \exp(-2\pi i\mathbf{k}_{oj}^{\text{sub}} \cdot \mathbf{r}) + D_{hj}^{\text{sub}} \exp(-2\pi i\mathbf{k}_{hj}^{\text{sub}} \cdot \mathbf{r})]. \quad (3)$$

The boundary conditions for wave amplitudes at the vacuum–epilayer interface are (Sakata & Hashizume, 1991)

$$E_0 + E_S = \sum_{j}^{4} D_{oj}^{\text{epi}}, \quad (4)$$

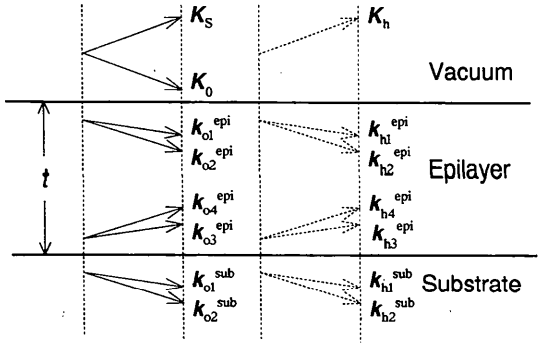

Fig. 1. Waves considered for an epilayer–substrate system in grazing-angle diffraction. Solid arrows show wave vectors in the incidence plane and broken arrows show out-of-plane wave vectors. Transmitted and diffracted wave vectors in the crystals, $\mathbf{k}_o$ and $\mathbf{k}_h$, have the same tangential components as their counterparts in vacuum.

$$E_h = \sum_{j}^{4} D_{hj}^{\text{epi}}, \quad (5)$$

$$K_{0\perp}(E_0 - E_S) = \sum_{j}^{4} k_{oj\perp}^{\text{epi}} D_{oj}^{\text{epi}}, \quad (6)$$

$$K_{h\perp}E_h = \sum_{j}^{4} k_{hj\perp}^{\text{epi}} D_{hj}^{\text{epi}}. \quad (7)$$

Equations (4)–(7) assume $D \simeq E$ in the epilayer. This assumption is justified because the dielectric constant of the crystal is very close to unity. At the film–substrate interface,

$$\sum_{j}^{4} D_{oj}^{\text{epi}} \exp(-2\pi i k_{oj\perp}^{\text{epi}} t) = \sum_{j}^{2} D_{oj}^{\text{sub}}, \quad (8)$$

$$\sum_{j}^{4} D_{hj}^{\text{epi}} \exp(-2\pi i k_{hj\perp}^{\text{epi}} t) = \sum_{j}^{2} D_{hj}^{\text{sub}}, \quad (9)$$

$$\sum_{j}^{4} k_{oj\perp}^{\text{epi}} D_{oj}^{\text{epi}} \exp(-2\pi i k_{oj\perp}^{\text{epi}} t) = \sum_{j}^{2} k_{oj\perp}^{\text{sub}} D_{oj}^{\text{sub}}, \quad (10)$$

$$\sum_{j}^{4} k_{hj\perp}^{\text{epi}} D_{hj}^{\text{epi}} \exp(-2\pi i k_{hj\perp}^{\text{epi}} t) = \sum_{j}^{2} k_{hj\perp}^{\text{sub}} D_{hj}^{\text{sub}}. \quad (11)$$

Subscript $\perp$ stands for the perpendicular components of the wave-number vectors. The film–substrate interface must be considered unless the film is much thicker than the X-ray penetration depth, which is of the order of 100 Å in our geometry. We assume that our system has the same lattice spacing in the surface direction in the substrate and the epilayer, $d^{\text{sub}} = d^{\text{epi}}$, and that there is a shift in the atom-plane position across the substrate–film interface. This is represented by parameter y for the displacement of the plane positions, parallel to the interface, in the epilayer from those in the substrate (Fig. 2). y is normalized by the lattice-plane spacing. $\mathbf{h}$ is the reciprocal-lattice vector considered, which is parallel to the interface. The displacement introduces phase shift $2\pi y$ in the Fourier coefficient of the dielectric susceptibility χ_h^{epi} for the epilayer:

$$\chi_h^{\text{epi}} = \chi_h' \exp(i2\pi y), \quad (12)$$

where χ_h' is the Fourier coefficient for a bulk crystal of the same material, calculated with the real-space origin placed at y apart from the origin used for the structure-factor calculation for the substrate crystal. Equation (12) is independent of origin choice for calculating χ_h^{epi}. For example, consider two origins at y or $y + s$ apart from the origin for calculating χ_h^{sub}. We obtain the same χ_h^{epi} since equation (12) indicates that χ_h' is multiplied by $\exp(i2\pi y)$ in the former case and that $(\chi_h')_{y+s} = \chi_h' \exp(-i2\pi s)$ is multiplied by $\exp[i2\pi(y + s)]$ in the latter case. Wave amplitudes in the epilayer and in the substrate, D_{oj} and D_{hj}, are related through the fundamental equation of dynamical theory:

$$D_{hj}/D_{oj} = [(k_{oj\perp}/K)^2 - \varphi_0^2 - \chi_0]/\chi_{\bar{h}}. \quad (13)$$

The above equation applies to the six pairs of amplitudes. k and χ should be respective values for the epilayer and the substrate.

There are 14 amplitudes to be solved for, 12 for the crystal waves and 2 for the vacuum waves. Once expressions (4)–(11) for the boundary conditions and the six equations arising from (13) are solved, all wave amplitudes are obtained. The X-ray field intensity $R(y', Z, y)$ in the epilayer at in-plane position y' and depth Z from the epilayer surface is written as follows:

$$R(y', Z, y) = \left| \sum_{j=1}^{4} D_{oj}^{\mathrm{epi}} \exp(-2\pi i k_{oj\perp}^{\mathrm{epi}} Z) + D_{hj}^{\mathrm{epi}} \exp(-2\pi i k_{hj\perp}^{\mathrm{epi}} Z) \exp[-2\pi i(y' + y)] \right|^2 . \tag{14}$$

Here, y' is defined relative to the film atomic planes (Fig. 2): $y' = 0.5$ corresponds to the halfway position between the adjacent atomic planes of the film. y and y' are positive when measured in the direction of **h**. Depth Z is defined to be positive in the epilayer and $Z = 0$ is located at the vacuum–epilayer interface.

Calculations were performed for a 100 Å-thick $Ca_{0.39}Sr_{0.61}F_2$ film on a GaAs(111) substrate in the symmetric $\bar{2}20$ reflection. The X-ray energy used is 18 keV. We consider three models of the film–substrate structure, *A*, *B* and *C*. In model *A*, there is no shift in the atom-plane position at the film–substrate interface, $y = 0$. Model *B* assumes a non-zero shift, $y \neq 0$. We assume that X-rays are diffracted by the thin film in both cases. The assumption is significant since the extinction distance of the film, 250 Å at the critical angle of incidence, is comparable with the film thickness 100 Å. We adopt the usual definition of the extinction distance, which is simplified to $\varphi_0\lambda/2|\chi_{hr}|$ at $\Delta\theta = 0$. λ is the X-ray wavelength. Furthermore, model *C* is introduced as an extreme case: it assumes a homogeneous electron density for the epilayer on a crystalline substrate. This means that no diffraction occurs in the film itself. X-rays are only refracted and absorbed in the medium.

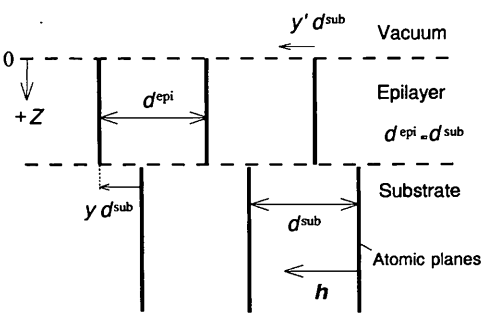

Fig. 2. Structure model for an epilayer–substrate system. Vertical atomic planes have an equal interplanar spacing $d^{\mathrm{sub}} = d^{\mathrm{epi}}$ but are displaced by yd^{sub} in the direction of the reciprocal-lattice vector **h**. y' is the coordinate defining the in-plane distance from the epilayer atomic planes. The Z axis is perpendicular to the surface with $+Z$ directed towards the crystal and $Z = 0$ located on the vacuum–epilayer interface.

Fig. 3 depicts a two-dimensional view of the X-ray field strength above and below the film surface for model *A*, calculated for the exact Bragg incidence, $\Delta\theta = 0$, and a glancing-incidence angle $\varphi_0 = 2.5$ mrad. This latter angle is greater than the critical angle for total external reflection for the film, φ_c^{epi}, which is 2.1 mrad at off-Bragg conditions. The field strength peaks slightly above the epilayer surface because 2.5 mrad > φ_c^{epi} and shows a nearly sinusoidal modulation along the y' direction. The intensity maxima are located slightly off the epilayer lattice planes at $y' = 0$ and 1. For $\Delta\theta < 0$, the field patterns have a peak around $y' = 0.5$ inside the epilayer, which is due to predominant field 2. For $\Delta\theta > 0$, a peak is located near $y' = 0$, where field 1 is more strongly excited than field 2. The field profiles look similar to those for a bare substrate except at $\Delta\theta < 0$. Wave fields 1 and 2 have separate critical angles $\varphi_{c1}^{\mathrm{epi}}$ and $\varphi_{c2}^{\mathrm{epi}}$, $\varphi_{c1}^{\mathrm{epi}} = 2.7$ and $\varphi_{c2}^{\mathrm{epi}} = 1.2$ mrad at $\Delta\theta = 0$. At $\Delta\theta < 0$, the stronger field 2 penetrates deep into the film, the interface is more important than at $\Delta\theta \geq 0$. Fig. 4 exhibits a field profile at $\Delta\theta = 0$ for model *B* with $y = 0.5$, where intensity maxima are located around $y' = 0.5$, which corresponds to the positions of the substrate lattice planes. The epilayer lattice planes are at $y' = 0$ and 1. The field modulation is larger here than in Fig. 3. In the vertical direction, the profile peaks near the epilayer–substrate boundary. The field profile for model *C* for $\Delta\theta = 0$ is similar to that for model *A*, but the modulation amplitude is smaller. Nevertheless, a y'-dependent field pattern is seen both in the non-crystalline film and above its surface. This indicates that the X-ray fields formed by the substrate penetrate through the film. For glancing-incidence angles sufficiently smaller than the critical angle of the film, the penetration depth is as small as 30 Å. The transmitted-wave intensity is strongly attenuated in the amorphous film and cannot reach the film–substrate boundary. In this case, the X-ray field above the film surface shows no modulation along the lateral direction for any incident angle θ.

Field behaviors depend on the model as described above. Fluorescence yield R_f from atoms located at relative position y' in the epilayer is expressed using the R of (14) as

$$R_f(y', y) = \sum_{n=0}^{N-1} \left\{ R(y', nd_v, y) f + \left[\left| \sum_{j=1}^{4} D_{oj}^{\mathrm{epi}} \exp(-2\pi i k_{oj\perp}^{\mathrm{epi}} nd_v) \right|^2 + \left[\left| \sum_{j=1}^{4} D_{hj}^{\mathrm{epi}} \exp(-2\pi i k_{hj\perp}^{\mathrm{epi}} nd_v) \right|^2 \right] (1 - f) \right\}, \tag{15}$$

where N is the total number of atom layers in the epilayer when counted along the surface normal and d_v is the epilayer spacing in this direction. f is called a coherent parameter, defined by

$$f = \left| \int_{-0.5}^{0.5} g(y') \exp(-2\pi i y')\, dy' \right|. \qquad (16)$$

Here, $g(y')$ is a distribution function for fluorescent atoms along **h**. $f = 1$ means perfectly ordered emissive atoms and $f = 0$ represents complete disorder. When $f = 0$, R_f is proportional to $|E_0 + E_S|^2 + |E_h|^2$. This expression is formally identical with that for adsorbed monolayers with $f = 0$ at the surface (Sakata & Hashizume, 1995). The only difference is that the secondary radiation from the film is proportional to the field strength integrated in the surface-normal direction.

We decomposed the field intensity into the components due to the four Bloch-wave fields in the epilayer for model A to examine the effects of the film–substrate boundary. The respective component intensities are sums of the field intensities at all (Ca, Sr)-atom-plane positions through the 100 Å thickness of the $CaSrF_2$ crystal. We note here that the (Ca, Sr) planes are sandwiched by the F planes of the fluorite structure in the [111] surface-normal direction. We adopted the T model, T(miss.) (Niwa, Sugiyama, Nakahata, Sakata & Hashizume, 1993), for the interface structure, in which substrate top-layer As atoms are missing, an F-atom layer is missing at the interface as well and the (111) lattice spacing is 0.73% larger in the film than in the substrate. Fig. 5(*a*) plots the component field intensities for $y' = y = 0$ and $\varphi_0 = 2.1$ mrad ($= \varphi_c^{epi}$) for the epilayer. Field 1 or 2, as defined above, is dominant at all $\Delta\theta$. The two profiles are not mirror related with respect to $\Delta\theta = 0$ because of the different dynamical absorptions for the two fields. It is notable that field 4 is stronger than field 3 at $\Delta\theta \leq 0$. The intensity resulting from an interference of these waves is negligibly small, which is not shown in Fig. 5(*a*). Separate calculations for $\varphi_0 = 2.5$ mrad indicate similar results of dominant field 1 and field 2 but, as to field 3 and field 4, the former field is stronger than the latter. We

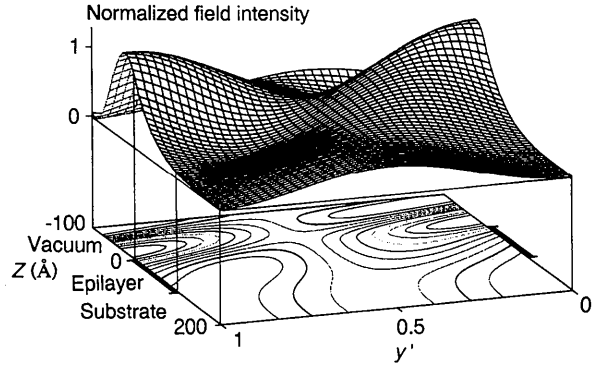

Fig. 3. Three-dimensional plot of the X-ray field intensities in the $y'Z$ plane. Calculated for a 100 Å-thick $Ca_{0.39}Sr_{0.61}F_2$ film on a GaAs(111) substrate under $\bar{2}20$ diffraction (model A: $y = 0$) with $\varphi_0 = 2.5$ mrad and $\Delta\theta = 0$ for 18 keV X-rays. The epilayer occupies $0 < Z < 100$ Å and the substrate occupies $Z > 100$ Å.

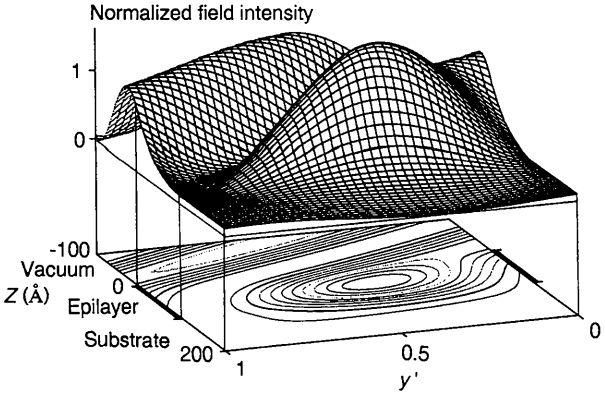

Fig. 4. Field intensity distribution for the same system as for Fig. 3 but of model B with $y = 0.5$.

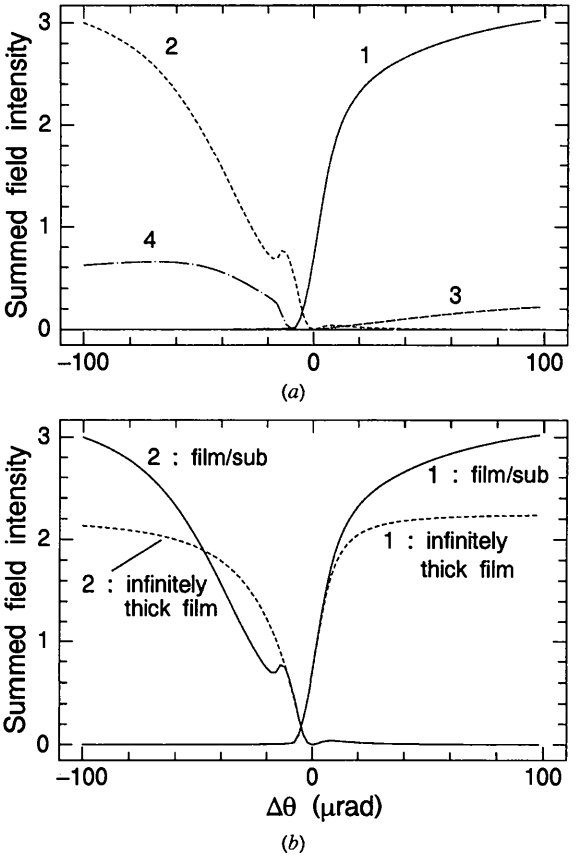

Fig. 5. (*a*) Decomposed field intensities for the 100 Å-thick epilayer. Labels represent the Bloch wave-field numbers. In (*b*), 'film/sub' denotes a 100 Å-thick (Ca, Sr)F_2 epilayer on a GaAs substrate (model A). 'Infinitely thick film' means a bulk $CaSrF_2$ crystal without a GaAs substrate. Calculated for $\varphi_0 = 2.1$ mrad.

note that fields 1, 2 and 4 are appreciable at $\varphi_0 \leq \varphi_c^{epi}$ and $\Delta\theta \leq 0$, whereas fields 1, 2 and 3 are intense at $\varphi_0 > \varphi_c^{epi}$. Field 2 shows a cusp at $\Delta\theta = -15$ μrad (Fig. 5*a*). This is due to field 4, reflection of field 2, generated with an appreciable amplitude at this angle. In an infinitely thick film, both fields 1 and 2 have smaller amplitudes than in the case of a 100 Å-thick film (Fig. 5*b*). Field 1 shows a similar behavior to that in the thin film but field 2 shows no cusp. It is to be noted that the standing-wave pattern due to fields 1 and 3 in the thin film has antinodes on the lattice planes, while the one due to fields 2 and 4 has nodes on the lattice planes. Fig. 5 shows that the angular profile of the total field is significantly affected by the presence of the boundary between the film and the substrate, even in model *A*.

Niwa, Sugiyama, Nakahata, Sakata & Hashizume (1993) propose the *T*(shift) model as a possible model of the $CaSrF_2$/GaAs(111) interface, where an F-atom layer is missing and As atoms are laterally shifted at the epilayer–substrate interface. The field behaviors for this model are very similar to those described above.

We mention two properties of the R_f profile. One is that the y'-dependent component of R_f for the epilayer–substrate system, $B_{film}(y', y)$, satisfies the same relation $B_{film}(y', y) = -B_{film}(y' + 0.5, y)$ as a bulk crystal (Sakata & Hashizume, 1995). The other is that, in our previous calculations for the $y = 0$ case (Sakata & Hashizume, 1991), the emission profiles for films with $t \leq 200$ Å at $\varphi_0 \leq \varphi_c^{epi}$ are distinct from those for films with $t > 200$ Å. Taken together with Fig. 5, this indicates that the X-ray field in a very thin film has a quite different intensity distribution from that in a bulk crystal.

Fig. 6 compares calculated Sr emission profiles for models *A* for $f = 1$ and *C* for the 100 Å-thick $CaSrF_2$ film. Profiles for model *C* are essentially damped profiles for a GaAs(111) surface with disordered Sr adsorbates. Profiles for model *A* show greater modulations than those for model *C*. At glancing angles φ_0 far from φ_c^{epi} (= 2.1 mrad), the two models exhibit qualitatively different emission profiles, which can be exploited for model distinction.

3. Sample and experimental

We briefly describe here the sample and experiment reported in Sakata, Kawamoto & Hashizume (1992). The sample is a $Ca_{0.39}Sr_{0.61}F_2$ film, epitaxially grown on a GaAs(111) substrate in a molecular-beam-epitaxy facility (Niwa, Sugiyama, Nakahata, Sakata & Hashizume, 1993). The alloy composition of the film was determined from the Rutherford back-scattering intensities observed from the Ca and Sr atoms in dummy samples. A fit to the X-ray specular reflectivity profile from the sample determined the film thickness at 99.9 (3) Å. Rocking-

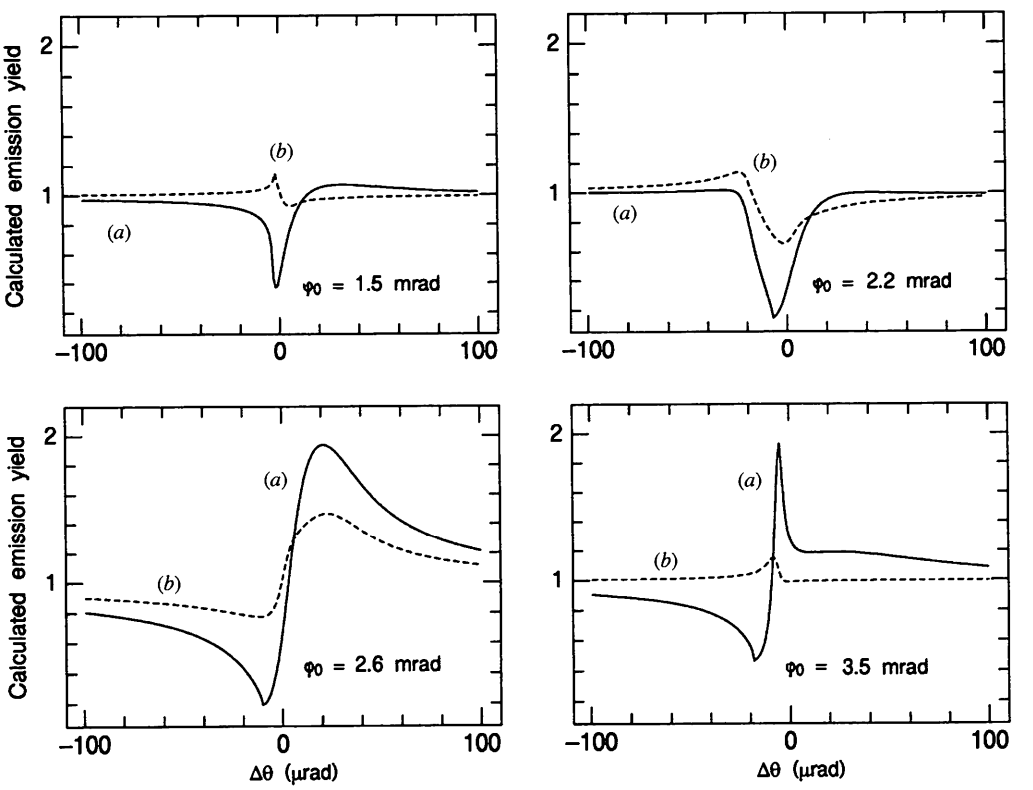

Fig. 6. Calculated Sr-emission yield for (*a*) model *A* with $f = 1$ and (*b*) model *C*.

curve measurements revealed a surface curvature of 3.5 mrad. Fits of the (111) X-ray standing-wave data indicated that the (111) lattice spacing, measured normal to the interface, is 0.73% larger in the film than in the substrate and that Sr atoms are ordered with a coherent fraction of 0.99 along the interface normal (Niwa, Sugiyama, Nakahata, Sakata & Hashizume, 1993). These results indicate that the film crystal is nearly perfect.

Experiments were carried out at the 14B vertical wiggler of the Tsukuba Photon Factory synchrotron source. The set-up was similar to that used in a previous experiment (Hashizume & Sakata, 1989). X-rays of 17.97 keV photon energy were extracted with a double-crystal silicon monochromator. A slightly dispersive Ge (220) collimator with an asymmetry factor of 0.016 was used and the obtained beam was guided onto the horizontally positioned sample at a grazing angle near the critical angle φ_c^{epi} (= 2.1 mrad). In addition, it nearly satisfied the Bragg condition for the ($\bar{2}20$) planes perpendicular to the surface. The substrate critical angle is φ_c^{sub} =2.5 mrad at the photon energy used. An energy-dispersive germanium detector, placed 5 mm above the sample surface, resolved the Sr K emission (14.2 keV) from the $Ca_{0.39}Sr_{0.61}F_2$ film.

4. Results and discussion

Fig. 7 compares the Sr emission intensities observed at $\varphi_0 = 3.3$ mrad with those calculated for $y = 0$, 0.25, 0.5 and 0.75 under the assumption that $y' = 0$, which may be natural because all lattice Sr atoms are located on the ($\bar{2}20$) diffracting planes in a perfect $CaSrF_2$ crystal. The calculations take into account the angular divergence $\delta\theta = 3.48$ μrad of the probing X-ray beam and the sample curvature $\delta\varphi = 3.5$ mrad. It is seen that the profiles are sensitive to the position y of the Sr-atom planes in the film, though strongly smeared. Different values for y give emission profiles with valleys and peaks in different positions relative to the center of the diffraction profile. This enables us to determine the lateral position of the epilayer atom planes relative to the substrate lattice. The curve for $y = 0$ is closest to the experimental data, but it shows a larger modulation than the data. This discrepancy will be explained by an introduction of coherent parameter f for the in-plane structure. Other curves may also fit the data when shifted horizontally. However, the smaller calculated modulation cannot be accounted for by practical values for the f parameter, which should be less than 1. The diffraction curve has a non-flat-top shape in spite of the asymmetry factor of 0.016 of the monochromator used, unlike the conventional Bragg case. This shape is intrinsic to the dynamical diffraction in grazing-incidence geometry but is not due to the sample curvature.

Fig. 8 compares the same Sr emission data with a calculation based on model C (amorphous film), which averages $R_f(y', y)$ over all y' and y. The calculated curve includes the X-ray divergence and the sample curvature, which average in effect the profiles shown in Fig. 6 over a range $\varphi_0 = 1.6$ to 5.1 mrad. Dominant contributions from off-φ_c^{epi} profiles make the modulation amplitude of the resultant curve quite small in disagreement with the observed profile.

In Fig. 9, we fit the emission data observed at various φ_0 angles using model B, including the X-ray divergence and the sample bending. The calculated profile for $\varphi_0 = 1.9$ mrad looks dissimilar to what is expected from those for $\varphi_0 = 1.5$ and 2.2 mrad in Fig. 6. Here again the sample curvature plays an important role. The results of the fits are summarized in Table 1, where y is very nearly equal to 0, indicating that the epilayer Sr planes are located on top of the ($\bar{2}20$) planes of the substrate GaAs, on which all Ga and As atoms are situated. $f \simeq 0.66$ shows that the film contains Sr atoms disordered in the in-plane direction. If we assume a Gaussian distribution function for the Sr atoms, this f value corresponds to $\sigma = 0.145 d_{220}$. Finite σ values can arise from thermal

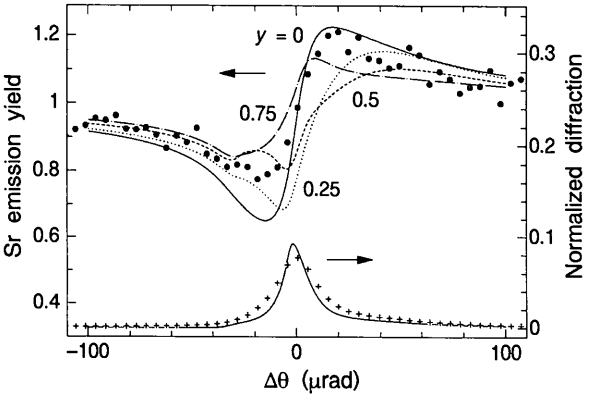

Fig. 7. Observed Sr emission signals (closed circles) and diffracted intensities (crosses) compared to calculated profiles for $y' = 0$, $y = 0$, 0.25, 0.5 and 0.75 at $\varphi_0 = 3.3$ mrad with $f = 1$. An experimental resolution function is included in the calculation.

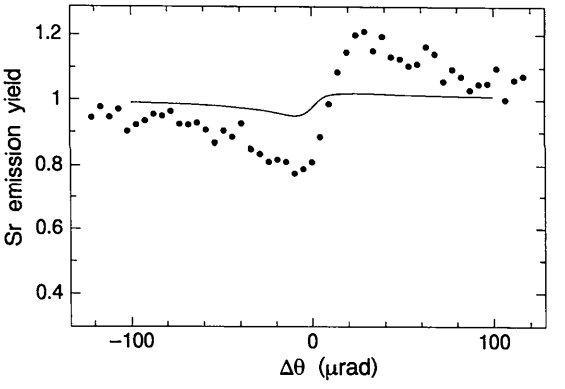

Fig. 8. The same emission data as in Fig. 7 compared to the calculation (line) for model C, smeared by the experimental resolution function.

Table 1. *Results of two-variable least-squares fits of the strontium emission profiles observed from a 100 Å-thick $Ca_{0.39}Sr_{0.61}F_2$ film on a GaAs (111) substrate*

All fits assume $y' = 0$. Numbers in parentheses are the estimated standard deviations in the least significant digit. R_w indicates weighted R factors.

φ_0 (mrad)	y	f	R_w
1.9	0.000 (10)	0.680 (32)	0.036
3.3	0.000 (13)	0.660 (20)	0.045
4.0	0.000 (8)	0.660 (9)	0.045
6.2	0.000 (5)	0.660 (12)	0.037

vibrations, interstitial atoms and depth-dependent atom positions in the epilayer film. For bulk GaAs and CaF_2, the isotropic mean displacements u of thermal vibrations are $u/d_{220} = 0.044$ and 0.045, respectively (Lonsdale, 1983). Atoms in a thin film may vibrate more vigorously than in the bulk, but the observed value of $\sigma = 0.145d_{220}$ is too large to be explained by thermal vibrations alone. The ionic radii of Ca, Sr and F are 0.99, 1.13 and 1.36 Å, respectively. $Ca_{0.39}Sr_{0.61}F_2$ with the fluorite structure has a large open space (*ca* 2.75 Å) along the diagonal of the unit cell, which can be occupied by interstitial Sr atoms. The conventional X-ray standing-wave data and crystal truncation data indicate a preference for a single domain (Niwa, Sugiyama, Nakahata, Sakata & Hashizume, 1993). The sample with several domains, with Sr atoms occupying different sites, *H*3, *T* and *T*4, on the substrate surface, would not make the f value low, as all these sites sit on the $(\bar{2}20)$ atomic plane. Let us assume that there is a continuous transition zone, where the Sr atoms occupy positions between sites, similar to the results for CaF_2/Si(111) (Huang, Zegenhagen, Philips & Patel, 1994). The small amount of the transition zone compared to the volume of the domains probably does not affect the degradation of the f value. Our assumption $d^{epi} = d^{sub}$, based on the lattice-matched design of the alloy composition $Ca_{0.39}Sr_{0.61}F_2$, is supported by only one peak being observed in a 1° angle range near the $\bar{2}20$ reciprocal-lattice point. A slightly lattice mismatched $Ca_{0.39}Sr_{0.61}F_2$ may, however, have been accommodated on the GaAs surface by introduction of dislocations at the interface, which can result in shifted Sr-atom positions. All these factors may contribute to the low f value observed. The data may be explained by a higher f value if a depth variation of the lattice spacing parallel to the interface is assumed for the film.

Niwa, Sugiyama, Nakahata, Sakata & Hashizume (1993) concluded that the Sr atoms in $Ca_{0.39}Sr_{0.61}F_2$ are more probably located in the *T* sites of the As surface of GaAs(111), rather than in the *T*4 sites. When projected onto the $(\bar{2}20)$ plane, the two structures show no difference. Sr atoms are located on top and halfway between the $(11\bar{2})$ atomic planes of the substrate GaAs. Hence, the two models cannot be distinguished with the

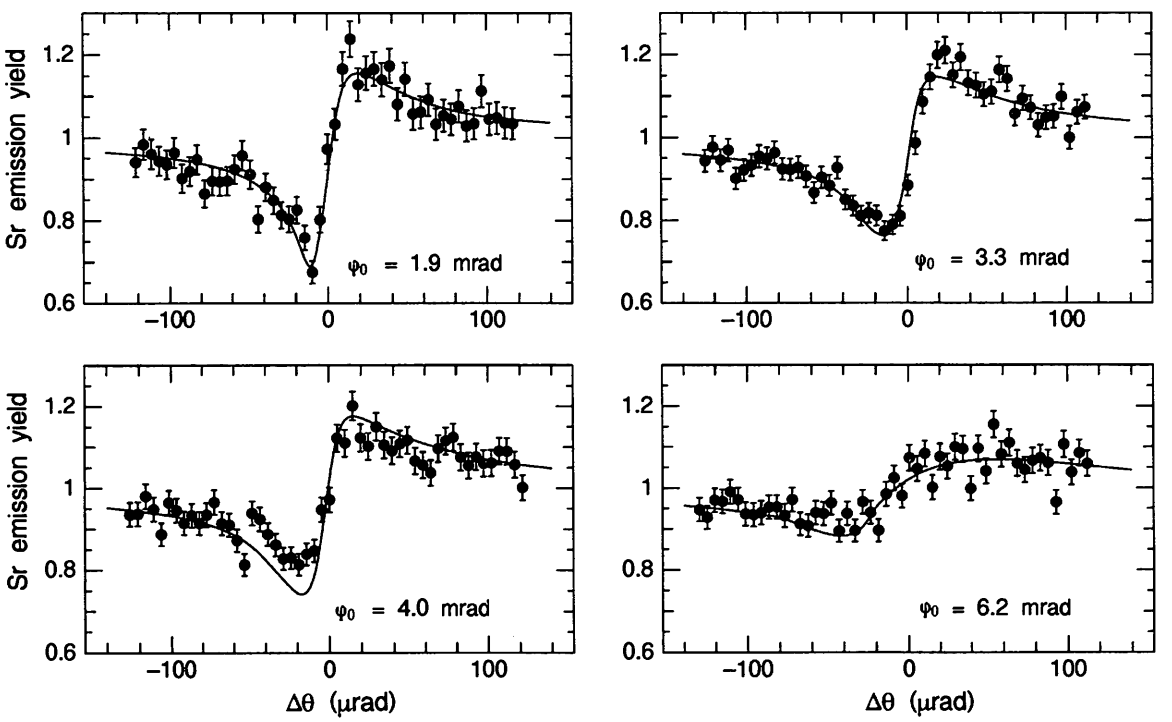

Fig. 9. Sr fluorescence signals (closed circles) fit to model *B*. Lines show fitted curves using y and f values assuming $y' = 0$ and include the experimental resolution function.

GAXSW technique using the $(22\bar{4})$ Bragg planes. This is also the case with other Bragg planes.

Finally, we suggest that the GAXSW technique is applicable to a film involving emissive atoms in two sites. Fig. 10 shows fluorescence profiles calculated for hypothetical films of thickness 100 Å having the $(\bar{2}20)$ planes at $y = 0$, 0.25, 0.5 and 0.75 and emissive atoms at $y' = -0.15$ and 0.15 on a GaAs substrate. It should not be hard to distinguish the four structures since the four profiles differ from each other as illustrated in Fig. 7.

The present work demonstrates that dynamical diffraction in crystalline overlayer films as thin as 100 Å must be considered in the grazing-angle geometry. We have shown that the technique is useful for the determination of the in-plane registration of film atoms with respect to substrate lattice atoms.

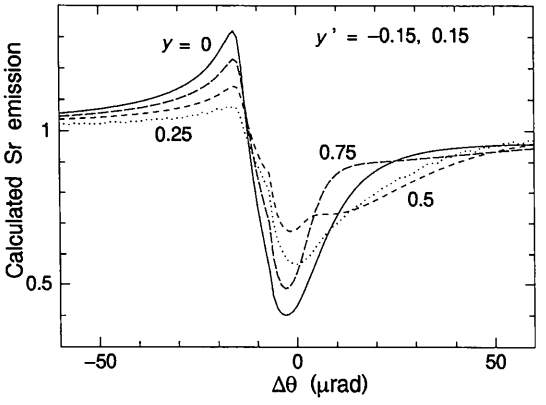

Fig. 10. Calculated Sr fluorescence profiles for four two-site structures with $f = 1$ on a GaAs (111) substrate for the $\bar{2}20$ diffraction. $\varphi_0 = 2.1$ mrad and 18 keV X-rays.

We thank I. Kawamoto for assistance in the experiments and P. M. Reimer for reading the manuscript. The synchrotron experiment was supported by the Photon Factory under proposal 90-106.

References

Aleksandrov, P. A., Afanasyev, A. M. & Stepanov, S. A. (1985). *Phys. Chem. Mech. Surf.* **3**, 2222–2240.

Cowan, P. L. (1985). *Phys. Rev. B*, **32**, 5437–5439.

Hashizume, H. & Sakata, O. (1989). *Rev. Sci. Instrum.* **60**, 2373–2375.

Huang, K. G., Zegenhagen, J., Philips, J. M. & Patel, J. R. (1994). *Phys. Rev. Lett.* **72**, 2430–2433.

Jach, T. & Bedzyk, M. J. (1990). *Phys. Rev. B*, **42**, 5399–5402.

Lonsdale, K. (1983). *International Tables for X-ray Crystallography*, Vol. III, edited by C. H. MacGillavry & G. D. Rieck, Section 3.3.5.1D. Dordrecht: Reidel.

Niwa, T., Sugiyama, M., Nakahata, T., Sakata, O. & Hashizume, H. (1993). *Surf. Sci.* **282**, 342–356.

Sakata, O. & Hashizume, H. (1991). Report of RLEMTIT, Vol. 16, pp. 27–38. Tokyo Institute of Technology, Yokohama, Japan.

Sakata, O. & Hashizume, H. (1995). *Acta Cryst.* A**51**, 375–384.

Sakata, O., Kawamoto, I. & Hashizume, H. (1992). The First Conference of the Asian Crystallographic Association, Abstract book, p. 16Q-8.